Met. Mater. Int., Vol. 17, No. 1 (2011), pp. 167~174
doi: 10.1007/s12540-011-0223-z Published 26 February 2011

Application of Direct Laser Melting to Restore Damaged Steel Dies

Jeong Hwan Jang, Byeong Don Joo, Sung Min Mun, Min Young Sung, and Young Hoon Moon*

School of Mechanical Engineering/Engineering Research Center for Net Shape and Die Manufacturing, Pusan National University, Busan 609-735, Korea

(received date: 17 May 2010 / accepted date: 7 October 2010)

Direct laser melting (DLM) technology can be applied to restore damaged steel dies. To understand the effects of DLM process parameters such as the laser power and scan rate, a series of experiments was conducted to determine the optimal operating parameters. To investigate the laser melting characteristics, the depth/height ratio, depth/width ratio and micro-hardness as a function of the laser energy density were analyzed. Fe-Cr and Fe-Ni layers were deposited on a steel die with 11.38 J/mm^2 of energy input. The wear-resistance and the friction coefficient of the deposited layer were investigated by a pin-on-disk test. The penetration depth decreased as the scan rate increased as a consequence of the shorter interaction time. The depth/height ratio of the deposited layer decreased with an increase in the scan rate. The depth/width ratio increased as laser power increased and the scan rate decreased. The deposition shape of the Fe-Ni powder was relatively shallow and wide compared with that of the Fe-Cr powder. The scan rate had a substantial effect upon the deposition height, with the Fe-Cr powder melting more than the Fe-Ni powder. The micro-hardness of the layer melted from the powders is higher than that of the substrate, and the hardness of the laser-surface-melted layer without any metal powder is higher compared to that of the metal-powder-melted layer. The direct laser melting process with Fe-Ni powder represents a superior method when restoring a steel die when the bead shape and hardness of the restored surface are important outcome considerations.

Keywords: direct laser melting (DLM), Fe-Ni powder, Fe-Cr powder, powder processing, melting, hardness test, wear

1. INTRODUCTION

Laser freeform fabrication can be applied to a range of industrial applications. Direct laser melting (DLM) technologies offer the advantages of single-stage production and geometric flexibility [1]. DLM technologies, which possess the capability to produce parts directly from metal powders, have been used to restore damaged mold surfaces. A three-dimensional component formed by DLM is built layer-by-layer. Each layer is melted by means of the direct laser melting of metal powders. Using a metal powder increases the size of the pool, which rapidly solidifies into a raised region when the laser moves on. The melted layer thus produced from metal powder can be precisely controlled. The advantage of DLM via partial melting is its ability to fabricate a fully densified metal part.

Laser surface hardening is suitable for applications that require a high level of hardness with a relatively shallow case depth on selected surface areas with no dimensional distortion. The automotive industry, in which wear resistance on certain surfaces is desired, has been one of the most important application areas for laser hardening [2]. Recent reviews of the principles and applications of laser treatments describe the use of lasers as a controlled heat source for transformation hardening [3-10]. These research results assist with evaluations of the feasibility of laser treatments for repair methods. In addition, repair methods that utilize laser melting have found a wide range of applications in a number of industries, including the aerospace and turbine industries for the repair of components or for the remanufacture of complete assemblies. Wang *et al.* [2] studied the influence of powder characteristics that included the mixture ratio, mean particle size and shapes, and size distribution on the energy absorption and on the features of the sintering zone. They observed that the penetration depth is highly dependent on the amount of energy absorbed by the powder bed. Cormier *et al.* [4] described the electron beam melting (EBM) process and presented results of microstructural analyses on H13 tool steel processed via EBM. Their study showed that the processing condition significantly affect the metallurgical properties. Zhang *et al.* [5] studied the effect of laser cladding alloy coating layers, and Pinkerton *et al.* [1] reported the use of diode laser direct metal deposition as a

*Corresponding author: yhmoon@pusan.ac.kr

means of repairing internal cracks in metallic components. Their assessment was done by repairing slots with rectangular and triangular cross-sections in H13 steel. The microstructure of laser surface-hardened hot-work tool steel was tempered martensite with a high hardness surrounded by a heat-affected zone of untempered martensite [1,6,7]. Rapid solidification is an effective method for the fabrication of metallic alloys with distinct properties for numerous industrial applications. Microstructural enhancement of the products is one of the main advantages of a rapid solidification process. The high cooling rate achievable during rapid solidification leads to significant refinement of the microstructure, which produces a remarkable improvement in the properties compared to those produced under conventional processes [11].

In the present work, DLM processes both with and without metal powders were implemented to investigate the effect of laser parameters on the quality of the repair. In the DLM process without powder, surface melting was performed by controlling the laser energy density (the laser power and the scan rate). In the case of DLM with metal powder, Fe-Cr and Fe-Ni layer depositions were deposited on a steel die at an energy input of 11.38 J/mm^2. The wear-resistance and the friction coefficient of the deposited layer were investigated by a pin-on-disk test. A number of different wear mechanisms frequently overlap and occur in a synergistic manner [12,13]. For the analysis of the die wear, this study focused on sliding wear.

2. DETAILS OF THE EXPERIMENT

2.1. Comparison of the surface melting area

Table 1 gives the chemical composition of the AISI H13 steel die used in this investigation.

To understand the effects of the process parameters of the laser power and scan rate on the DLM process, a series of experiments was conducted to determine the optimal parameters. The component properties are strongly influenced by the molten pool size, which is mainly controlled by the laser energy input. Hence, it is important to analyze the surface melting area. To conduct these analyses, two different experiments were conducted. One experiment used a heat source (a fiber laser beam) on a steel die substrate without metal powder to analyze the surface melted area. The other experiment used laser melting with metal powder (Fe-Cr and Fe-Ni powders) for an analysis of the deposited layer on the steel die substrate by single-track melting with different laser processing parameters.

Table 1. Chemical compositions of AISI H13 (wt.%)

Fe	Cr	Ni	Mo	Si	V	Mn	C
Bal.	5.2	1.3	1.23	1.12	1.1	0.41	0.41

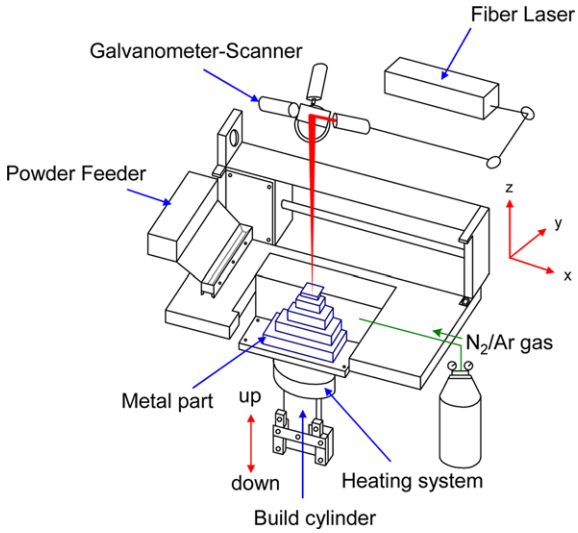

Fig. 1. Schematic drawing of Direct Laser Melting system.

In the laser beam melting experiments, a fiber laser beam with a diameter of 0.08 mm was used. The laser-melted layer was fabricated with a laser power of 50 W to 200 W and a scan rate of 3.66 mm/s to 366.22 mm/s. Figure 1 shows an illustration of the apparatus used for the laser surface treatment. The radiation source is a YLR-200 CW Ytterbium fiber laser manufactured by IPG Photonics with a maximum power P of 200 W, a wavelength λ of 1075 nm and a laser beam diameter d of 0.08 mm in the focal position. A scanner by Scanlab (hurrySCAN®20) was used to control the laser scanning method. To produce an oxide-free coating, the chamber was shielded using argon gas (5 *l*/min) in all experiments. The vertical movement of the cylinder was driven by a motor.

To analyze a laser-melted layer produced with metal powder, Fe-Cr and Fe-Ni powders were laser-melted at an energy input ranging from 1.7 J/mm^2 to 683 J/mm^2. Table 2 gives the chemical composition of the Fe-Cr powder and the Fe-Ni powder. These powder particles had a spherical shape with an average diameter of 20 μm.

2.2. Wear test

The experiments were conducted using a pin-on-disk (POD) test apparatus. During the tests, a data logging system continuously recorded the test time (sliding distance), the

Table 2. Chemical compositions of metal powder (wt.%)

Powder	Fe	Ni	Cr	Al	Si	Cu	C	Mo	S	Mn
Fe-Ni	Bal.	15.7	3.96	0.76	0.72	0.32	2.07	0.12	0.24	-
Fe-Cr	Bal.	7.6	18.2	0.70	0.60	0.30	2.27	0.20	-	1.2

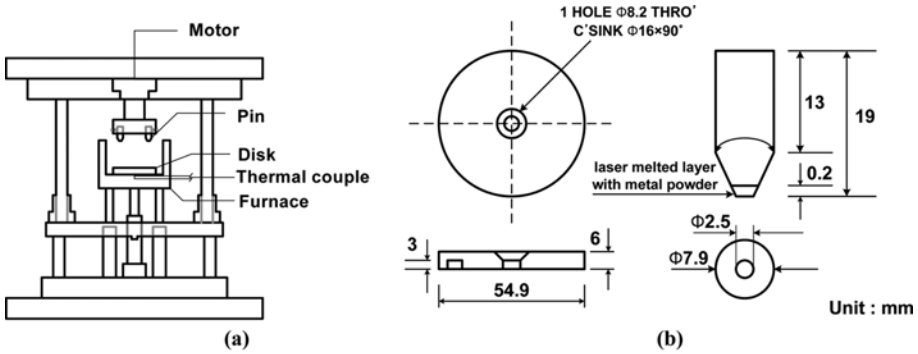

Fig. 2. Pin-on-disk test: (a) test system and (b) dimensions of the disk and the pin.

friction coefficient, the torque and the normal force. The data were written to a file for further processing. The disks had a diameter of 54.9 mm and a height of 6 mm. The disk was machined from H13 die steel of which the hardness was approximately 200 HV. The pin was shaped so that the disks could be firmly mounted, and the disks had a circular contact area with a diameter of 2.5 mm. The average surface roughness of both the pin and the disk after NC-machining was 0.3 μm to 0.4 μm. Figure 2 shows the dimensions of the disk and the pin. The contact surfaces of the pin were a melted layer with a thickness of approximately 0.2 mm formulated with the Fe-Ni and the Fe-Cr powders using an energy input of 11.38 J/mm^2 (a laser power of 200 W and a scan rate of 219.73 mm/s). To measure the wear rate and friction, a wear test was carried out using a POD testing system under a varying load (20 N, 40 N and 60 N) at a sliding speed of 200 rpm. Prior to the test, the pin and the disk were cleaned in an ultrasonic cleaner. Following the test run, the pin and the disk were removed from the test apparatus and cleaned again. The weight of the pin was then measured by an electronic balance with a resolution of 0.1 mg [14].

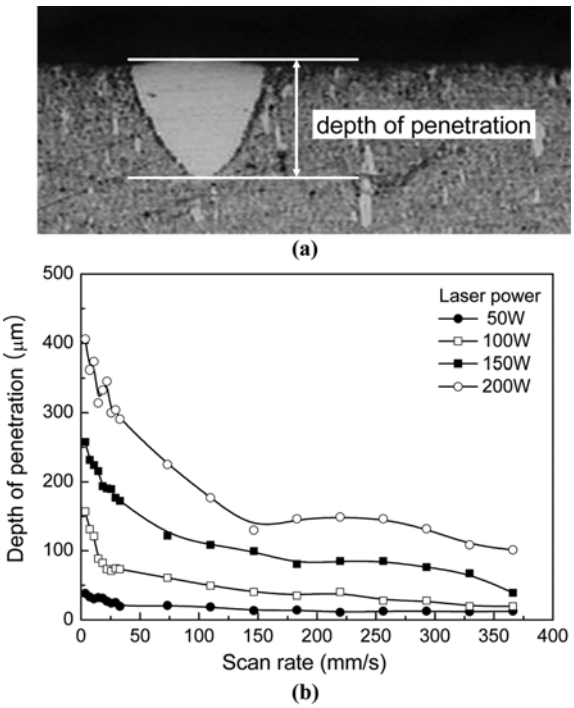

Fig. 3. Properties of the surface melting area: (a) cross-sectional view and (b) depth of penetration on the surface versus the scan rate for various laser powers.

3. RESULTS AND DISCUSSION

3.1. Properties of the surface melting area without metal powder

Figure 3 shows the depth of penetration on the substrate surface versus the scan rate for various laser powers. The results obtained for a particular melting application will depend on the specific energy density as determined by the laser power and scan rate. The accumulated energy on the substrate surface decreases with an increase in the scan rate, which results in a non-linear decrease in the depth of penetration.

Figure 4 shows the depth of penetration versus the laser energy density for various laser powers. This figure shows the deepest penetration possible with current technology, not necessarily the optimum penetration conditions. The discontinuity in the curve near 0 J/mm^2 to 50 J/mm^2 may represent the transition from conduction melting to deep penetration by the keyhole mode [10]. The laser energy density can be estimated by

$$\text{Laser energy density} = \frac{P \cdot \tau \cdot f}{d \cdot v} \text{ (J/mm}^2\text{)} \quad (1)$$

where P is the laser power (W), v is the scan rate (mm/s), τ is the pulse duration (s), f is the pulse frequency (Hz) and d is the beam diameter (mm). The laser power and the scan rate were varied in this study. The other operational parameters in Eq. 1 were fixed as follows: a beam diameter of 0.08 mm, a pulse frequency of 50 kHz and a pulse duration of 20 μs.

Figure 5 shows the depth of penetration (z) as a function of the parameter $P/\sqrt{dv}$ using a regression analysis of the experimental data. Steen and Courtney [15] reported a simi-

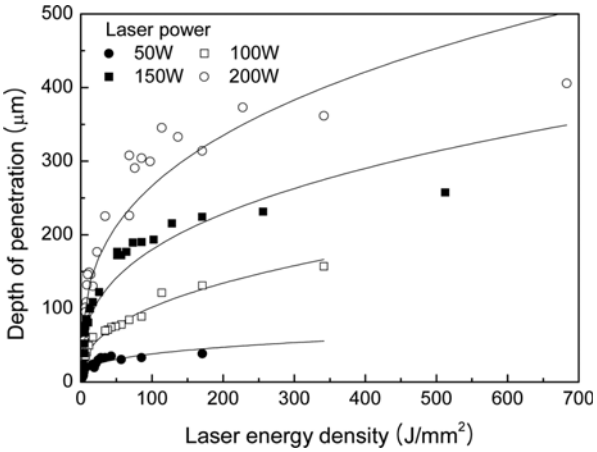

Fig. 4. Depth of penetration versus the laser energy density for various laser powers.

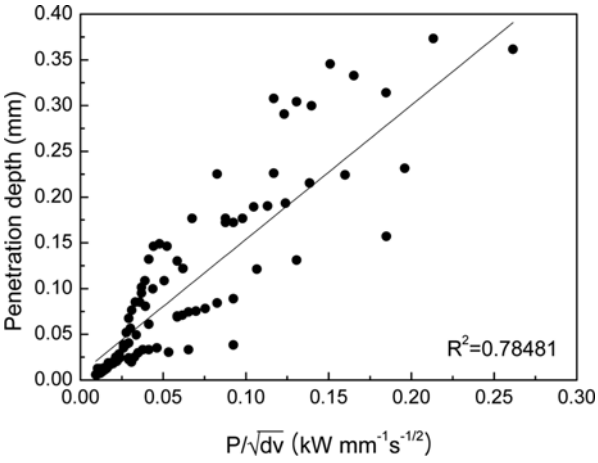

Fig. 5. Variation of the parameter $P/\sqrt{dv}$ with the depth of penetration, z after Steen and Courtney.

lar relationship for the penetration depth z. This figure shows that the scatter of this parameter with the depth of penetration is quite significant, with the scatter increasing as the penetration depth increases. The regression analysis gives

$$z = 0.00715 + 1.46701 P/\sqrt{dv} \quad (2)$$

where z is the depth of penetration (mm), P is the laser power (kW), v is the scan rate (mm/s) and d is the beam diameter (mm). The correlation coefficient (R^2) in Eq. 2 is 0.78481.

The influence of the operating laser parameters can be explained as follows. An increase in the scan rate decreases the depth of penetration (z), as an increase in the speed decreases z as a consequence of the shorter interaction time and thermal gradient, allowing insufficient time for the molten metal to penetrate deeply into the substrate. However, an increase in the laser power increases the surface power density. Hence, the depth of penetration will reach a greater depth for this type of heat treatment [6,16].

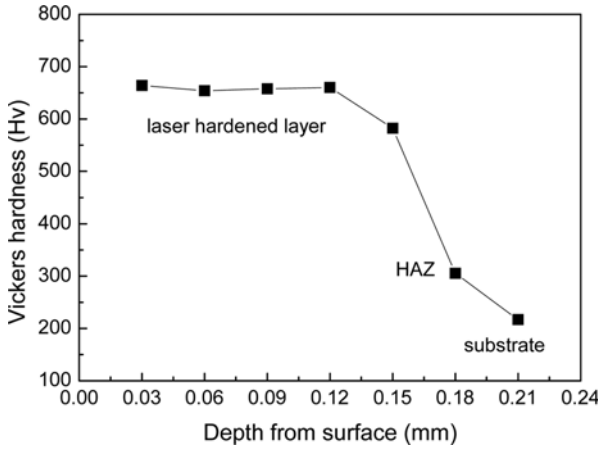

Fig. 6. Dependence between micro-hardness and depth of hardening; P = 200 W and v = 219.73 mm/s.

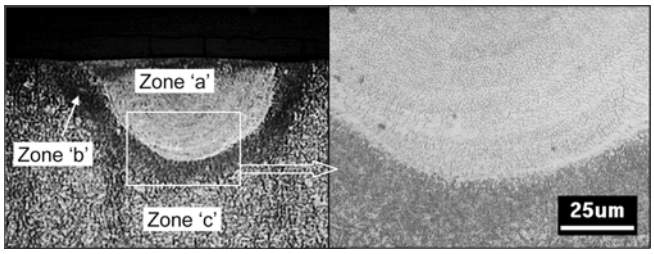

Fig. 7. Micro-structure in the transverse cross-section of laser-melting specimen made of the steel die, P = 200 W, v = 219.73 mm/s, E = 11.38 J/mm^2.

Figure 6 shows the change in the micro-hardness as a function of the depth at a laser power of 200 W and a scan rate of 219.73 mm/s. Figure 7 shows the microstructure of the characteristic zones after laser surface melting. This microstructure is from the specimen with an energy input to 11.38 J/mm^2. Based on the analysis of the microstructure shown in Fig. 7, three characteristic zones can be distinguished: zone 'a' is where a melted layer begins to solidify. The cooling rate in the liquid is very high as a result of self-cooling from the substrate, and a dendritic structure forms with a micro-hardness of 581 HV to 670 HV. Zone 'b' is the heat-affected zone (HAZ), a transition zone between the melted region and the parent metal with a fine-grained ferritic-pearlitic microstructure. The micro-hardness of this zone is about 305 HV. In zone 'c', the structure of the substrate was not affected by the laser, showing a micro-hardness of 217 HV.

3.2. Properties of the surface melted area with metal powder

Figure 8 shows cross-sectioned beads of the surface melted area with the metal powder at various scan rates.

Figure 8(a) shows the results when the heat intensity generated by the laser was too high, causing the metal powder and part of the steel substrate to vaporize. The beads in Fig.

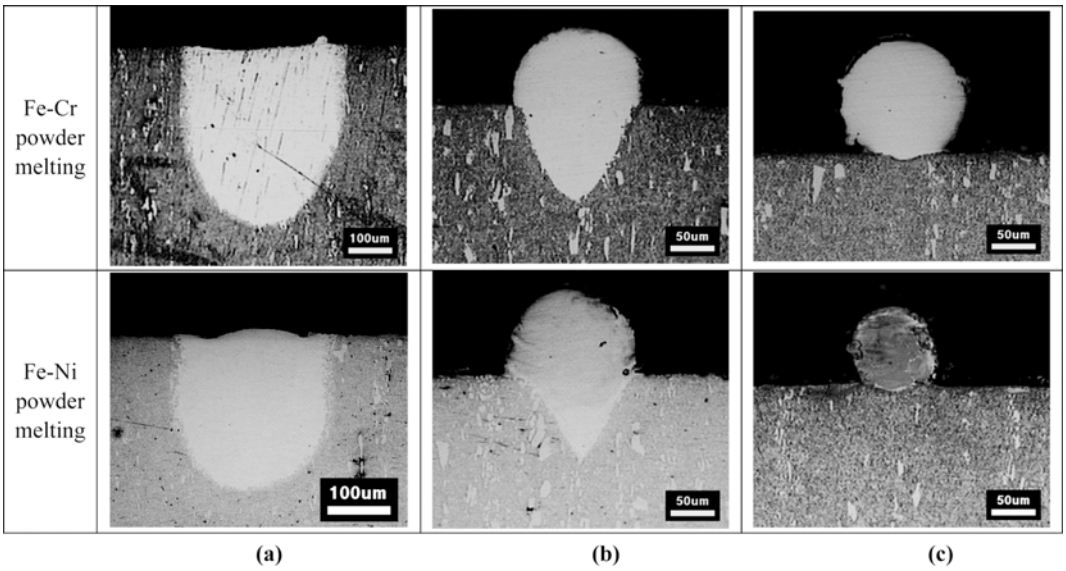

Fig. 8. Cross-sectioned beads: (a) partial vaporization, (b) full melting and (c) insufficient bonding.

8(a) were formed under a laser power of 200 W and a scan rate of 36.6 mm/s. When deposition occurs at this level of heat intensity, a deep melt shape is formed and the high pressures lead to material removal by melt expulsion [17,18]. Figure 8(b) shows the conditions in which the heat generated allowed for full melting to the substrate with good wetting characteristics. The beads in Fig. 8(b) formed under a laser power of 150 W and a scan rate of 73.2 mm/s. Figure 8(c) shows beads with insufficient bonding. The insufficient bonding resulted from an insufficient heat energy supply. Insufficient bonding occurs with a laser power of 100 W and a scan rate of 109.9 mm/s.

In the single-scan experiments a process operating window was obtained, as plotted in Fig. 9. Figure 9 shows that lower scan rates at higher laser powers cause vaporization as compared to higher scan rates. This is a result of greater heat intensities being generated at lower scan rates. In contrast, insufficient bonding was observed at lower laser powers and higher scan rates due to the insufficient supply of the heat energy.

The shape of the melted bead can be characterized by the melting width (W), the melting height (H) and the melting depth (D), as defined in the melting profile shown in Fig. 10(a). The limits of the scan rate are the full melting ranges shown in Fig. 9. Figures 10(b) and (c) show the results of the single-track melting experiments. As shown in Fig. 10(b), the depth/height ratio of the melting layer decreases with an increase in the scan rate. An important operating criterion is to estimate whether or not the scan rate and the laser power are appropriate for the process. If the ratio is too large, too much material from the previous layers can be remelted during subsequent laser scanning, causing irregularities in the melted shape. On the other hand, too small a ratio will

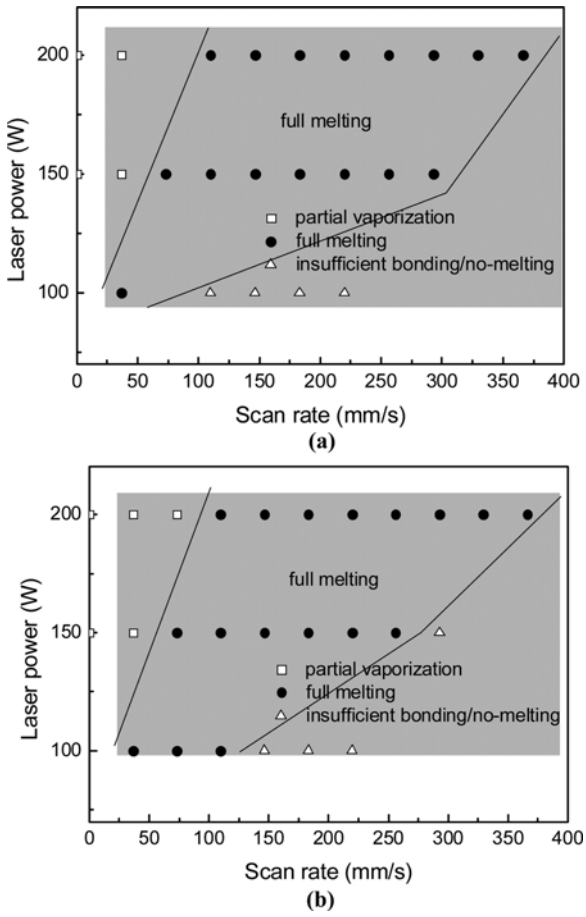

Fig. 9. Process operating window for full melting: (a) Fe-Cr powder and (b) Fe-Ni powder.

decrease the bonding strength between the neighboring layers because the molten pool energy is insufficient to re-melt

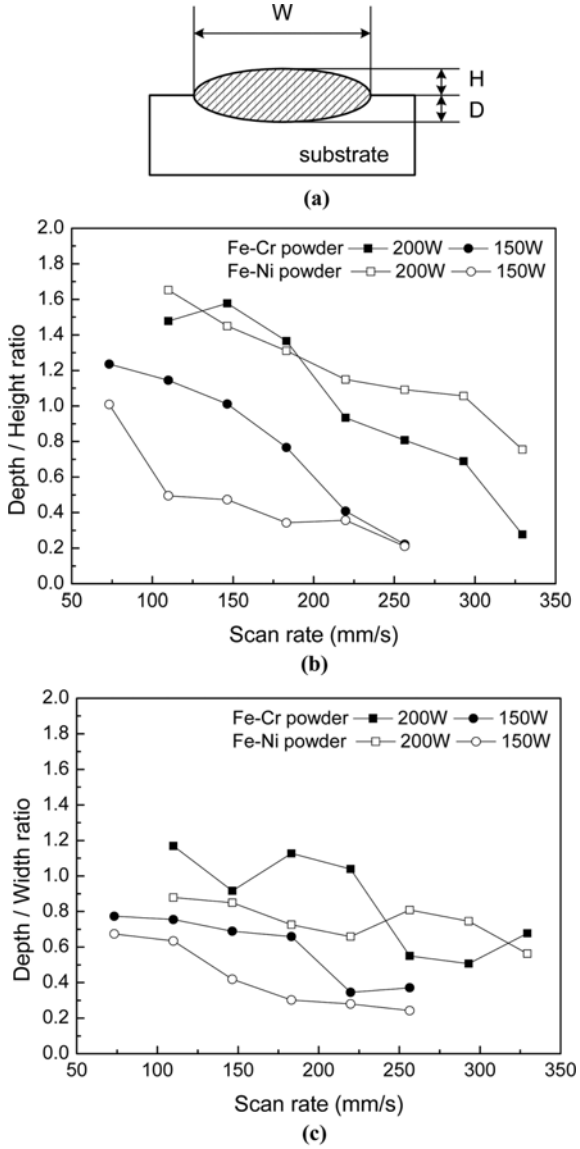

Fig. 10. Influence of the scan rate on the melting width, height and depth in the DLM process: (a) melting profile, (b) depth/height ratio and (c) depth/width ratio.

an adequate amount of existing material [19]. For the Fe-Cr powder melting test, as the scan rates increased, the resulting deposited height becomes higher compared to when Fe-Ni powder is melted at the same penetration depth. This height difference indicates that the scan rate has a substantial effect on the deposited height upon melting with Fe-Cr powder. For the Fe-Ni powder melting test, the difference in the depth/height ratio as a function of the laser power is larger as compared to melting with the Fe-Cr powder under the same scan conditions. This shows that the laser power has a greater effect upon melting with the Fe-Ni powder compared to when the Fe-Cr powder was used.

Figure 10(c) shows the depth/width ratio as a function of the scan rate for two laser powers. The depth/width ratio at a laser power of 200 W is higher than that at a laser power of 150 W. This ratio is higher upon a higher laser power and is higher as well at lower scan rates. For the Fe-Ni powder, the bead shape is relatively shallow compared to the Fe-Cr powder. That is, the melting depth with the Fe-Cr powder is deeper than it is with the Fe-Ni powder under the same melting conditions.

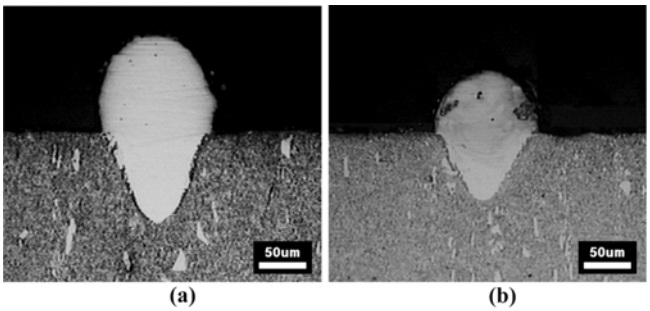

Fig. 11. Desired melting shape using 200 W power and 219.7 mm/s scan rate: (a) the Fe-Cr powder and (b) the Fe-Ni powder.

Considering the results shown in Figs. 8, 9, and 10, it is highly recommend to use the following conditions to achieve a good bead shape with a depth/height and depth/width of approximately 1.0 [20]: a laser power of 200 W and a scan rate of 219.7 mm/s. Figure 11 shows the results of the melting shape with the Fe-Cr powder and the Fe-Ni powder using the recommended conditions.

Figure 12 shows the micro-hardness distribution of the laser melted layer. The measured points were from the melted bead center to the substrate in the horizontal direction. The micro-hardness of the Fe-Ni powder bead is higher than that of the Fe-Cr powder. The profile can be divided into three regions: the melted layer, the heat affected zone (HAZ) and the substrate. The higher hardness of the laser melted layer compared to the substrate is attributed to the rapid solidification of the melt pool and the concentrated heating of the laser beam.

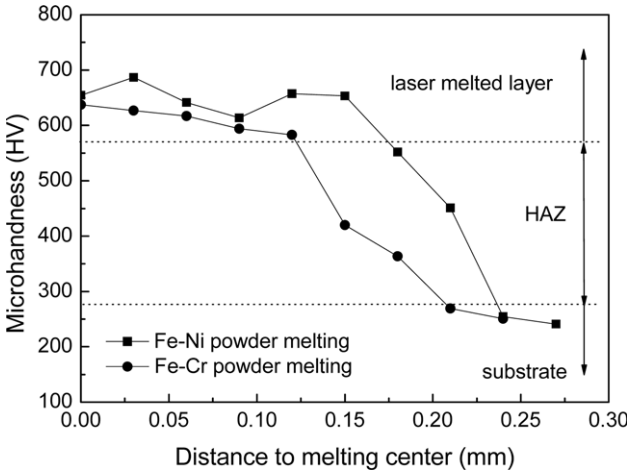

Fig. 12. Micro-hardness of the laser melted layer.

3.3. Wear characteristics of the laser melted layers

Figure 13 shows the variation in the friction coefficient with the sliding distance at a normal force of 60 N. The graph clearly shows two distinct regions of interest: running-in, and stable sliding. Running-in takes place during the early stage of the test during in which the friction coefficient is unstable, usually rising from a low value to a value above average and then decreasing to a stable sliding condition at a certain sliding distance [21-24].

Figure 14 shows that the friction coefficient is between 0.1 and 0.3. As the normal load is increased, a higher friction coefficient is obtained. The laser-melted layer melted with the Fe-Ni powder shows a lower friction coefficient than that with the Fe-Cr powder. The friction coefficient was calculated by measuring the torque on the pin and the radius of the wear track and then using the following equation:

$$\mu = \frac{T}{F_N \cdot r} \tag{3}$$

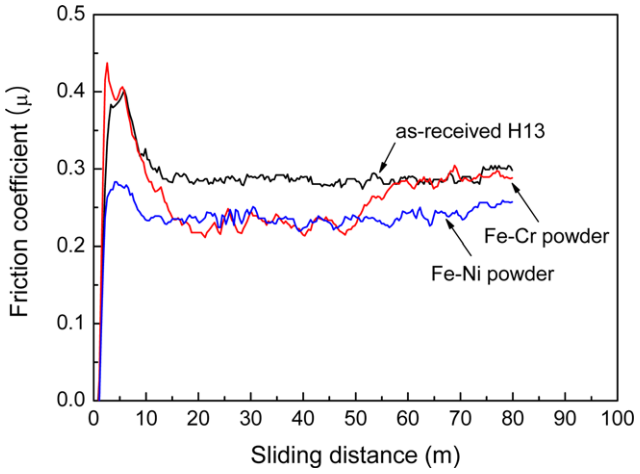

Fig. 13. Representative runs showing the variation friction coefficient at load of 60 N.

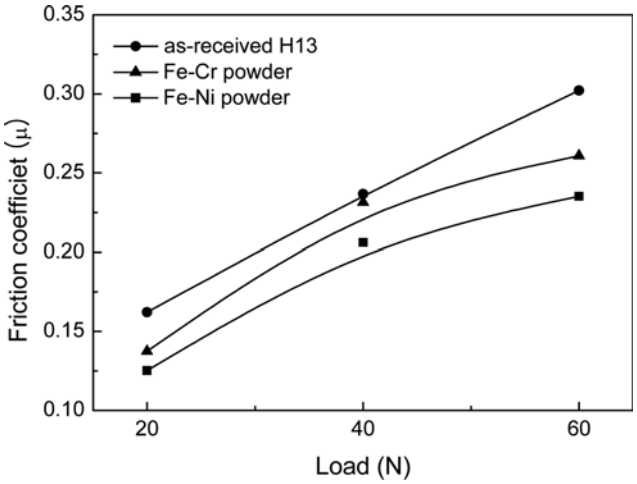

Fig. 14. Comparison of the friction coefficient.

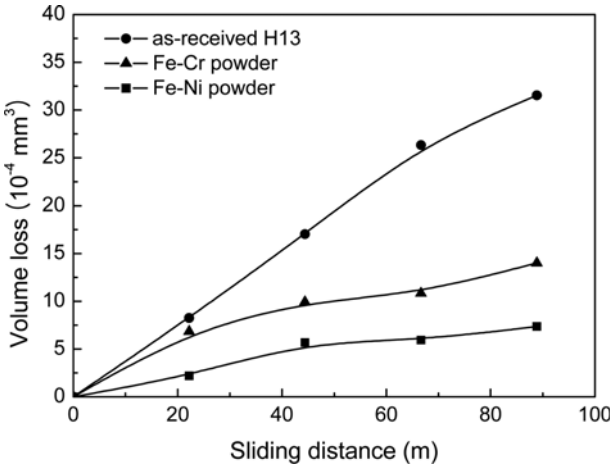

Fig. 15. Changes in volume loss with an increase in sliding distance at a constant applied load of 40 N.

In Eq. 3, μ is the friction coefficient, T is the torque, F_N is the applied load, and r is the radius of the wear track.

The wear resistance measurements were taken from untreated surfaces and compared with surfaces produced with the metal powders. Wear is expressed as the amount of wear volume on the pin.

Figure 15 shows the relationship between the wear volume losses as a function of the sliding distance. The results show that the as-received H13 exhibits high wear, which increases in severity as the sliding distance increases. In contrast, the laser-melted surfaces melted with the Fe-Ni powder and with the Fe-Cr powder show excellent wear resistance and a modest increase in the amount of volume loss as the sliding distance increases. For the as-received H13, the volume loss was particularly severe during the initial 'running in' stage of wear. In comparison, the laser melting test showed mild wear behavior as the sliding distance increased. The wear tests also revealed that surfaces melted with the Fe-Ni powder resulted in the most wear-resistant surfaces. This wear resistance was further confirmed by comparing the wear rates with the various loads shown in Fig. 16. The results indicate the lowest wear rate for surfaces melted with the Fe-Ni powder and the highest wear rate for the as-received H13.

The wear rate was calculated using the wear volume and the sliding distance. The variations in the wear rate as a function of the sliding distance at loads of 20 N, 40 N and 60 N are shown in Fig. 16. The findings show that the influence of the load on the wear rate is strongest for the as-received H13 tool steel. These results show that severe wear occurs for the as-received H13, but after surface melting with the metal powder, mild wear occurs due to the change in the surface. The increase in surface hardness after melting reduces the wear rate. The laser melting process with the Fe-Ni powder is desirable for restoring a steel die when the bead shape and wear resistance of the restored surface are considered.

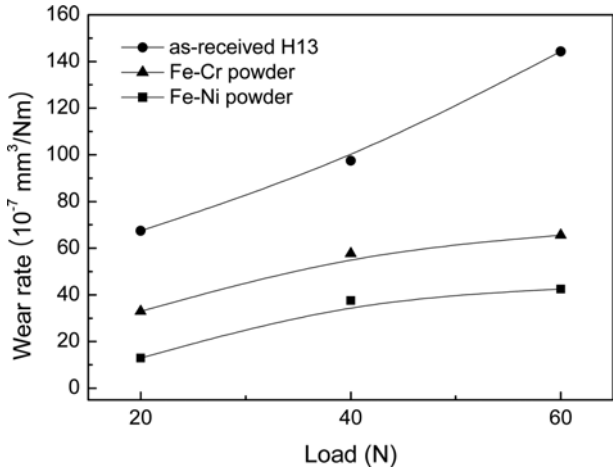

Fig. 16. Comparison of the wear rate.

4. CONCLUSIONS

On the basis of the mechanical properties and microstructural experimental studies and the results obtained regarding the effect of the direct laser melting (DLM) process on a steel die, the following conclusions may be drawn:

(1) The depth of penetration was found to be closely related to the parameters as suggested by Steen and Courtney. A higher laser power was favorable for producing the highest depth of penetration. An increase in the scan rate had a negative influence on the depth of penetration.

(2) The depth/height ratio of the melted layer decreases with an increase in the scan rate. The depth/width ratio increases with an increase in the laser power and a decrease in the scan rate.

(3) The scan rate has a substantial effect upon the deposited height with the Fe-Cr powder more than it does with the Fe-Ni powder. The deposition depth of the Fe-Ni powder is significantly affected by the laser power compared to that of the Fe-Cr powder.

(4) The melting depth of the Fe-Cr powder is deeper than that of the Fe-Ni powder under the same melting conditions. As a result, the bead shape of the Fe-Ni powder is relatively shallow and wide compared to that of the Fe-Cr powder.

(5) The direct laser melting process with Fe-Ni powder is recommended to restore a steel die when the bead shape and wear resistance of the restored surface are considered.

ACKNOWLEDGMENTS

This research was partially supported by Basic Science Research Program through the National Research Foundation of Korea (NRF) funded by the Ministry of Education, Science and Technology (KRF-2007-521-D00206) and NCRC (National Core Research Center) program through the National Research Foundation of Korea funded by the Ministry of Science and Technology (2010-0008-276).

REFERENCES

1. A. J. Pinkerton and L. Li, *Int. J. Adv. Manuf. Technol.* **25**, 471 (2005).
2. X. C. Wang, T. Laoui, J. Bonse, J. P. Kruth, B. Lauwers, and L. Froyen, *Int. J. Adv. Manuf. Technol.* **19**, 351 (2002).
3. H. Y. Lee, T. J. Kim, and Y. J. Cho, *J. Kor. Inst. Met. & Mater.* **47**, 267 (2009).
4. D. Cormier, O. Harrysson, and H. West, *Rapid Prototyping J.* **10**, 35 (2004).
5. S. H. Zhang, M. X. Li, T. Y. Cho, J. H. Yoon, W. Fang, Y. K. Joo, J. H. Kang, and C. G. Lee, *Met. Mater. Int.* **14**, 315 (2008).
6. R. Komanduri and Z. B. Hou, *Inter. J. Heat Mass Transfer* **44**, 2845 (2001).
7. K. A. Chiang and Y. C. Chen, *Mater. Lett.* **59**, 1919 (2005).
8. J. Grum and J. M. Slabe, *Appl. Surf. Sci.* **208-209**, 424 (2003).
9. A. J. Pinkerton, W. Wang, and L. Li, *Proc. Inst. Mech. Eng. Part B J. Eng. Manuf.* **222**, 827 (2008).
10. X. B. Liu, M. Pang, Z. G. Zhang, W. J. Ning, C. Y. Zheng, and G. Yu, *Opt. Lasers Eng.* **45**, 929 (2007).
11. M. Rajabi, M. Vahidi, A. Simchi, and P. Davami, *Mater. Charact.* **60**, 1370 (2009).
12. M. H. Jones and D. Scott, *Industrial Tribology: The Practical Aspects of Friction, Lubrication and Wear*, Elsevier Scientific Publishing Company, New York (1983).
13. J. A. Williams, *Tribol. Int*. **38**, 863 (2005).
14. J. H. Jang, B. D. Joo, J. H. Lee, and Y. H. Moon, *Met. Mater. Int.* **15**, 903 (2009).
15. W. M. Steen and C. H. G. Courtney, *Metals Technol.* **6**, 456 (1979).
16. R. Sagaro, J. S. Ceballos, A. Blanco, and J. Mascarell, *Wear* **225-229**, 575 (1999).
17. K. A. Mumtaz, P. Erasenthiran, and N. Hopkinson, *J. Mater. Process. Technol.* **195**, 77 (2008).
18. J. P. Kruth, L. Froyen, J. Van Vaerenbergh, P. Mercelis, M. Rombouts, and B. Lauwers, *J. Mater. Process. Technol.* **149**, 616 (2004).
19. L. Peng, Y. Taiping, L. Sheng, L. Dongsheng, H. Qianwu, X. Weihao, and Z. Xiaoyan, *Int. J. Mach. Tools Manuf.* **45**, 1288 (2005).
20. E. Capello and B. Previtali, *J. Mater. Process. Technol.* **174**, 223 (2006).
21. M. F. Jensen, J. Bøttiger, H. H. Reitz, and M. E. Benzon, *Wear* **253**, 1044 (2002).
22. H. So, *Wear* **184**, 161 (1995).
23. B. Y. Choi and H. K. Kim, *J. Kor. Inst. Met. & Mater.* **47**, 667 (2009).
24. D. J. Ha, H. K. Sung, J. W. Park, and S. H. Lee, *J. Kor. Inst. Met. & Mater.* **47**, 406 (2009).